

## Electronic Supplementary Information

### What defines the perovskite solar cell efficiency and stability: fullerene-based ETL structure or film morphology?

Mohamed M. Elnaggar,<sup>a,b</sup> Alexander V. Mumyatov,<sup>a</sup> Nikita A. Emelianov,<sup>a</sup> Lavrenty G. Gutsev,<sup>a,c</sup> Victoria V. Ozerova,<sup>a</sup> Ivan V. Fedyanin,<sup>d,e</sup> Yulia V. Nelyubina,<sup>a,d</sup> Sergey I. Troyanov,<sup>f</sup> Bala R. Ramachandran,<sup>c</sup> and Pavel A. Troshin<sup>g,h,a,\*</sup>

<sup>a</sup> Federal Research Center of Problems of Chemical Physics and Medicinal Chemistry, Russian Academy of Sciences (FRC PCP MC RAS), Semenov prospect 1, 141432 Chernogolovka, Moscow Region, Russian Federation

<sup>b</sup> Department of Physics, Faculty of Science, Tanta University, 31512 Tanta, Egypt

<sup>c</sup> Institute for Micromanufacturing, Louisiana Tech University, Ruston, LA 71272, United States

<sup>d</sup> A. N. Nesmeyanov Institute of Organoelement Compounds of Russian Academy of Sciences, Vavilova st. 28, bld. 1, Moscow, 119991, Russian Federation

<sup>e</sup> Plekhanov Russian University of Economics, Stremyanny per. 36, Moscow, 117997, Russian Federation

<sup>f</sup> Chemistry Department, Moscow State University, Russian Federation

<sup>g</sup> Harbin Institute of Technology, 92 West Dazhi Street, Nan Gang District, Harbin, Heilongjiang Province, China

<sup>h</sup> Zhengzhou Research Institute of HIT, 26 Longyuan East 7th, Jinshui District, Zhengzhou, Henan Province, 450000, China

\* Corresponding author: troshin2003@inbox.ru

#### Contents:

Experimental	2
Theoretical calculations	4
Device fabrication	7
Device characterization	8
Charge carrier mobility measurements in OFETs	8
FigureS1. Current density–voltage characteristics (left) and EQE spectra (right) for Cs <sub>0.12</sub> FA <sub>0.88</sub> PbI <sub>3</sub> -based PSCs with different ETLs ( <b>F1</b> , <b>F4</b> , <b>F5</b> , and <b>F6</b> ).	10
Figure S2. A. Dimer configuration taken from experimental crystals (pentagon-edge) and molecular dynamics minimum (edge-edge). The dotted blue line indicates the distance between the centroids of fullerenes, the red dotted line shows the shortest distance between fullerene surfaces. B. Averaged radial pair distribution function of C <sub>60</sub> . C. Molecular dynamics simulations with a target temperature of 300 K run for 20 ps. CR stands for charge recombination.	11
Figure S3. PL spectra of Cs <sub>0.12</sub> FA <sub>0.88</sub> PbI <sub>3</sub> films before and after deposition of different fullerene derivatives used as ETL materials.	12
Figure S4. Normalized parameters: (a) open circuit voltage, (b) short circuit current density, and (c) FF for PSCs assembled using different fullerene-based ETLs and exposed to aging under continuous light illumination.	13
Figure S5. FTIR spectra of Cs <sub>0.12</sub> FA <sub>0.88</sub> PbI <sub>3</sub> and fullerene-based ETLs with marked bands used for IR s-SNOM measurements.	14

## **Experimental:**

**Materials:** Anhydrous isopropyl alcohol (IPA) (Sigma–Aldrich), DMF (Sigma-Aldrich), anhydrous NMP (Sigma- Aldrich), anhydrous toluene (Sigma-Aldrich), anhydrous chlorobenzene (CB, Sigma-Aldrich), PbI<sub>2</sub> (Sigma-Aldrich), methylammonium iodide (MAI, Sigma-Aldrich), formamidinium iodide (FAI, Sigma-Aldrich), Caesium iodide (CsI, Sigma-Aldrich) and PTAA (Ossila) were used as received.

**Instrumentation:** Steady-state PL spectra were measured under a nitrogen atmosphere using an ocean Insight QE Pro spectrometer and a 450 nm laser as the excitation source. NMR spectra were recorded using AVANCE III Bruker NMR spectrometer (proton Larmor frequency is 500 MHz) and Bruker AVANCE 600 NMR spectrometer (proton Larmor frequency is 600 MHz). FTIR spectra were recorded using PerkingElmer FT-IR Spectrometer Spectrum 100. The IR s-SNOM measurements were performed in inert atmosphere inside nitrogen-filled glove box using neaSNOM (Neaspec) in PsHet mode. VIT\_P/Pt cantilevers (NT-MDT) with Pt tip coating, a probe radius of 25 – 35 nm, a typical resonance frequency of around 300 kHz and a force constant of 50 N/m were used for the measurements.

## **Synthesis of derivatives of fullerenes:**

The fullerene derivatives (**F1-F6**) were synthesized using the modified procedure reported previously.<sup>S1-S4</sup> A corresponding tosylhydrazone (1.3 eq.) was dissolved in 5 mL of dry pyridine in a dried three-necked flask provided with Ar inlet, a thermometer, and a magnetic stirring bar. Then, NaOMe (1.3 eq.) was added, and the mixture was stirred during 15 min. A solution of fullerene in 100 mL of HPLC grade 1,2-DCB was added, and the homogeneous reaction mixture was stirred at 65-70 °C during 7 h. Then reaction mixture was heated at reflux for about 8 h. (The course of the reaction was

followed by TLC (SiO<sub>2</sub>/toluene.) After filtration, the solvents were removed under reduced pressure. The residue was purified by flash column chromatography with petroleum ether-CS<sub>2</sub>, and petroleum ether - toluene in variable ratio as eluents (from 4:1 to 1:1).

**Compound F1:** Yield: 28%. The spectral data were reported previously.<sup>S2</sup>

**Compound F2:** Yield: 37%. <sup>1</sup>H NMR (500 MHz, CDCl<sub>3</sub>, δ, ppm, *J*, Hz): 7.49 (d, *J* = 8.6, 1H), 6.77 (d, *J* = 8.6, 1H), 4.23 (s, 3H, OCH<sub>3</sub>), 4.14 – 3.99 (m, 2H, OCH<sub>2</sub>), 3.93 (s, 3H, OCH<sub>3</sub>), 2.49 (s, 3H, CCH<sub>3</sub>), 1.82 – 1.71 (m, 2H, OCH<sub>2</sub>CH<sub>2</sub>), 1.55-1.45 (m, 2H, CH<sub>2</sub>CH<sub>3</sub>), 0.96 (t, *J* = 7.4, 3H, terminal CH<sub>3</sub>). <sup>13</sup>C NMR (126 MHz, CDCl<sub>3</sub>, δ, ppm): 154.33, 153.21, 150.35, 146.36, 146.26, 145.76, 145.31, 145.29, 145.23, 145.20, 145.15, 145.10, 144.97, 144.94, 144.86, 144.82, 144.77, 144.59, 144.58, 144.45, 144.43, 144.08, 144.02, 144.00, 143.97, 143.88, 143.82, 143.18, 143.17, 143.11, 143.10, 143.08, 143.07, 143.06, 143.01, 142.56, 142.51, 142.50, 142.39, 142.33, 142.31, 142.28, 142.18, 141.35, 141.17, 140.98, 140.97, 140.68, 138.31, 138.08, 136.51, 126.92, 124.00, 106.24, 82.39, 79.69, 73.33, 61.86, 56.11, 44.22, 32.31, 20.95, 19.35, 14.10. MS (ESI): [M]<sup>-</sup> calculated for C<sub>74</sub>H<sub>20</sub>O<sub>3</sub> m/z 956 found m/z 956.

**Compound F3.** Yield: 45%. The spectral data were reported previously.<sup>S2</sup>

**Compound F4.** Yield: 46%. The spectral data were reported previously.<sup>S3</sup>

**Compound F5.** Yield: 20%. <sup>1</sup>H NMR (600 MHz, CDCl<sub>3</sub>, δ, ppm): 7.91 (d, 2H), 7.50 (m, 3H), 5.15 (s, 2H), 3.20 (t, 2H), 2.84 (t, 2H). <sup>19</sup>F NMR (282 MHz, CDCl<sub>3</sub>, δ, ppm): 140.3 (m, 2F), 151.4 (t, 1F), 160.2 (m, 2F). <sup>13</sup>C NMR (CS<sub>2</sub>-acetone-D<sub>6</sub>, 150 MHz, δ, ppm): 31.34, 50.76, 53.22, 79.47, 125.53, 128.41, 128.64, 128.76, 129.12, 132.14, 135.98, 137.81, 138.26, 140.86, 141.13, 142.08, 142.22, 142.28, 143.04, 143.09, 143.14, 143.17, 143.82, 144.22, 144.58, 144.74, 144.85, 145.07, 145.15, 145.26, 145.82, 147.33, 148.41, 170.34.

**Compound F6.** <sup>1</sup>H NMR (500 MHz, CDCl<sub>3</sub>+CS<sub>2</sub>, δ, ppm): δ 8.07 – 8.03 (m, 2H), 7.72 – 7.68 (m, 1H), 2.58 (s, 3H), 0.35 (s, 18H). <sup>13</sup>C NMR (126 MHz, CDCl<sub>3</sub>+CS<sub>2</sub>, δ, ppm): 150.02,

149.23, 147.03, 146.20, 146.17, 146.13, 146.03, 145.90, 145.83, 145.78, 145.66, 145.46, 145.39, 144.94, 144.77, 144.12, 144.06, 144.01, 143.97, 143.94, 143.32, 143.17, 143.08, 141.97, 141.77, 140.86, 139.03, 138.76, 138.58, 138.51, 137.62, 81.82, 49.21, 23.54, 0.00.

### **X-ray crystallography:**

Synchrotron X-ray data for **F2** and **F5** were collected at 100 K on BL14.2 at the BESSY storage ring (Berlin, Germany) using a MAR225 detector ( $\lambda = 0.84344$  and  $0.9050$  Å, respectively). The data for **F6** were collected on a Bruker APEX DUO diffractometer ( $\lambda(\text{CuK}\alpha) = 1.54178$  Å,  $\varphi$ - and  $\omega$ -scans). The structures were solved by a direct method with the SHELXS program<sup>S5</sup> (**F2** and **F5**) and a dual-space method with the SHELXT program<sup>S6</sup> (**F6**) and refined on  $F^2$  in an anisotropic approximation with the SHELXL program.<sup>S7</sup> Hydrogen atoms were placed in calculated positions and refined in a riding model. Crystallographic data have been deposited with the Cambridge Crystallographic Data Center, CCDC 2250001 (**F5**), 2250002 (**F2**) and 2252121 (**F6**). The data could be accessed free of charge from <https://www.ccdc.cam.ac.uk/structures/>.

### **Theoretical Calculations:**

To obtain the theoretical redox potentials and reorganization energy of C<sub>60</sub>, the other functionalized fullerenes) and PCBM we performed DFT calculations of the neutral and ionic species in the Gaussian 16 suite of programs.<sup>S8</sup> These optimization were performed with the widely-employed B3LYP<sup>S9</sup> functional, the reorganization energy was calculated with the long-range corrected meta-GGA  $\omega$ B97XD functional<sup>S10</sup> which includes the Grimme D2 dispersion correction.<sup>S11</sup> Initial relaxations were performed with the Gaussian 3-21G basis set<sup>S12</sup> then the basis sets were improved to 6-31G\*; a final single point calculation was performed with the 6-31+G\* basis set. This choice of functionals was justified by their previous successful usage in

fullerene charge transfer calculations.<sup>S13</sup> In situations where convergence was difficult, we applied Gaussian's orbital shifting option until convergence was achieved. The RMS force threshold was set to  $3 \times 10^{-4} \text{ eV/\AA}$  and the total energy threshold to  $10^{-8} \text{ a.u.}$  The reorganization potential was defined as:

$$E_{red} = E^- - E^0 \#(S1)$$

Where  $E^-$  is the energy of the fully relaxed negatively charged species and  $E^0$  is the neutral. The reorganization energy was calculated as:

$$\lambda = (E_*^- - E^-) + (E_*^0 - E^0) \#(S2)$$

Where  $E_*^-$  is the anionic energy at the neutral geometry and  $E_*^0$  is the neutral energy at the anionic geometry both of which were obtained by single-point calculations. To ensure the validity of our methodology we compared  $\lambda$  of fullerene and found that it is in concordance with previous calculations<sup>S14</sup> where the calculated electron transfer rate was in decent agreement with experimental values. We chose HOMO and LUMO levels from PBE/6-311G\* calculations since this method previously showed the best agreement with experimental levels for functionalized fullerenes.<sup>S15</sup>

The electron transfer integral  $J_{ij}$ , which is the leading term in the Marcus equation, was calculated via the dimer method (DFT/DIPRO).<sup>S16</sup> The CATNIP Integral package<sup>S17</sup> was interfaced with Gaussian16 for this task. Two types of dimers were prepared:

1. The coordinates were obtained from experimentally obtained crystallographic coordinates and optimized using the Vienna Ab Initio Simulation Package (VASP)<sup>S18</sup> of programs. For calculations involving VASP, we utilized the PBE generalized gradient approximation (GGA) and a D3 dispersion correction<sup>S19</sup> and the Projector augmented-wave (PAW) pseudopotentials.<sup>S20,S21</sup> After optimizations were completed, we performed single point evaluations of the electronic structure with the strongly

constrained and appropriately normed (SCAN) meta-GGA functional.<sup>S22</sup> We increased the number of k-points in the first Brillouin zone via Monkhorst-Pack grid generation<sup>S23</sup> up to 3x3x3 for C<sub>60</sub> and similarly for other fullerenes. We generally neglected **F4** and **F5** in our calculations due to the fact that **F4** includes a chloro-benzene ring in the lattice while **F5** has a perfluorobenzene, the former makes it difficult to evaluate and compare  $\lambda$  while fluorinated benzenes have, as we previously found,<sup>S24</sup> a strong functional dependence. As such we limited our calculations to HOMO and LUMO for these fullerenes.

2. Dimers were obtained by running the optimized geometries obtained in the previous part in a DFTB-MD simulation. Our simulations were performed on a timescale of 20 picoseconds, a time step of 1 femtosecond, and utilizing a Nose-Hoover thermostat with a target temperature of 300 K. We utilized a coupling strength of 1600 cm<sup>-1</sup> and also included Lennard-Jones potentials to account for dispersion.<sup>S25</sup>

Since the functionalized fullerenes are utilized as ETL's in the photovoltaic stack the electron mobility of the material is of particular importance. The electron mobility may be estimated within a fullerene dimer pair via the semiclassical Marcus theory, which is valid for temperatures above 100 K ( $kT \gg \hbar\omega$ ):

$$\omega_{ij} = \frac{|J_{ij}|^2}{\hbar} \sqrt{\frac{\pi}{\lambda kT}} \exp\left[-\frac{(-\Delta G_{ij} + \lambda)^2}{4\lambda kT}\right] \#(S3)$$

Where  $J_{ij}$  is the electron transfer integral (when between LUMO's) or the charge recombination integral (when between HOMO-LUMO),  $\lambda$  is the intramolecular reorganization energy where we neglect the intermolecular component, it can also be interpreted as corresponding to the local electron-phonon coupling and  $\Delta G_{ij}$  is the driving force which in a donor-acceptor pair is estimated as the difference of electron affinities. Electron transfer between fullerenes is optimal when the  $J_{ij}$  is large while  $\lambda$  is small, the latter generally holds true for these systems due to the

rigidity of the fullerene core.<sup>S26</sup> The transfer integral; however, can change by orders of magnitude based on the arrangement of the charge-transfer dimer. In the case of planar organic semiconductors,<sup>S16</sup> configurations which are degenerate or near-degenerate in energy can have a very large difference in  $J_{ij}$ , similarly, this term can also greatly vary in the case of fullerenes<sup>S27</sup> since nuclear motion greatly affects this term.

### **Device Fabrication:**

The indium tin oxide (ITO) substrates ( $2.5 \times 2.5 \text{ cm}^2$ ) were ultrasonically cleaned with deionized water, acetone, and isopropanol for 5 min each. Then, the substrates were dried with a stream of nitrogen and subjected to oxygen plasma treatment for 10 min. Afterward, all substrates transferred to a nitrogen-filled glovebox for depositing all functional layers. PTAA was spin-coated on ITO at 4000 rpm for 30 s, followed by thermal annealing at 100 °C for 10 min.

The perovskite precursor solution was prepared by dissolving 1.5 M  $\text{PbI}_2$  (691.5 mg), 0.18 M CsI (46.7 mg), and 1.32 M FAI (227.0 mg) in DMF: DMSO solvent mixture (4: 1 by vol., 800 : 200  $\mu\text{L}$ ). The perovskite precursor solution (70  $\mu\text{l}$ ) was spin-coated atop glass/ITO/PTAA substrate at 4000 rpm for 20 s with dripping 100  $\mu\text{l}$  of chlorobenzene (CB) as anti-solvent 20 after start of the spin-coating program. The deposited films were annealed at 100 °C for 10 min.

Afterward, the ETL material ( $\text{PC}_{61}\text{BM}$  or **F1–F6**) was deposited on the perovskite films by spin coating from CB or  $\text{CB}:\text{CS}_2$  solutions within 30 s (optimal material concentrations and spin-coating frequencies are given in Table 1 in the main text). All used solutions were filtered through a 0.4  $\mu\text{m}$  pore size poly(tetrafluoroethylene) (PTFE) filter.

### **Device characterization:**

The current-voltage characteristics of the solar cells were measured in an inert nitrogen atmosphere inside a glove box using the simulated AM1.5G illumination ( $100 \text{ mW cm}^{-2}$ ) provided by a K. H. Steuernagel Lichttechnik GmbH solar simulator and a shadow mask with the aperture of  $0.07 \text{ cm}^2$ . The intensity of the illumination was checked before each measurement using a calibrated silicon diode with a known spectral response. The J–V curves were recorded using Advantest 6240A source-measurement units in forward and reverse directions with the scan rate of  $10 \text{ mV s}^{-1}$  at the temperature of  $25 \text{ }^\circ\text{C}$ . The EQE spectra were measured under anoxic nitrogen atmosphere using a LOMO (Russia) instrument equipped with 150 W xenon lamp as a light source for generation of monochromatic illumination for the measured cells with the step of 5 nm.

The aging experiments were performed using continuous LED illumination providing approximately the same dose of absorbed photons as the standard  $100 \text{ mW cm}^{-2}$  AM1.5G light flux. The equilibrium temperature on the sample surface was  $43.5 \pm 2.5 \text{ }^\circ\text{C}$ . All devices were tested under open circuit conditions. All tests were performed under anoxic conditions inside nitrogen glove box, which could be considered as a model of an “ideal encapsulation”.

### **Charge carrier mobility measurements in OFETs**

Glass substrates ( $1.5 \times 1.5 \text{ cm}^2$  in size) were cleaned for 5 min in air plasma (40 kHz, 150 W). Aluminum gate electrodes (100 nm thick) were deposited onto the cleaned glass substrates by thermal evaporating in high vacuum ( $10^{-6}$  mbar) using a shadow mask. The electrochemical oxidation of aluminum was performed in a solution of citric acid (2.8 g per 50 mL of distilled water) for 360 s at the bias voltage of 30 V to form the dielectric oxide layer. Thin films of fullerene derivatives (n-type semiconductor materials) were deposited directly atop  $\text{AlO}_x$  inside the MBraun glove box under nitrogen ( $\text{H}_2\text{O}$ ,  $\text{O}_2 < 0.1 \text{ ppm}$ ) by spin-coating from solutions. The concentration of **F1-F5** and **PC<sub>61</sub>BM** in chlorobenzene was  $25 \text{ mg mL}^{-1}$ . Compound **F6** was spin-coated

from carbon disulfide ( $25 \text{ mg mL}^{-1}$ ) due to its limited solubility in chlorobenzene. The substrate rotation speed was 1500 rpm for all compounds. Next, silver source and drain electrodes were deposited by resistive thermal evaporation in high vacuum ( $10^{-6}$  mbar) using a shadow mask. The transistor channel length (L) was  $50 \text{ }\mu\text{m}$ , and the width (W) was 2 mm. The capacitance of  $\text{AlO}_x$  layer was  $4.53 \times 10^{-8} \text{ F cm}^{-2}$ . The transistor characteristics were measured using a Keithley 2612A dual-channel voltage and current source-meter. The mobility of charge carriers was calculated from I-V curves in the saturation regime.

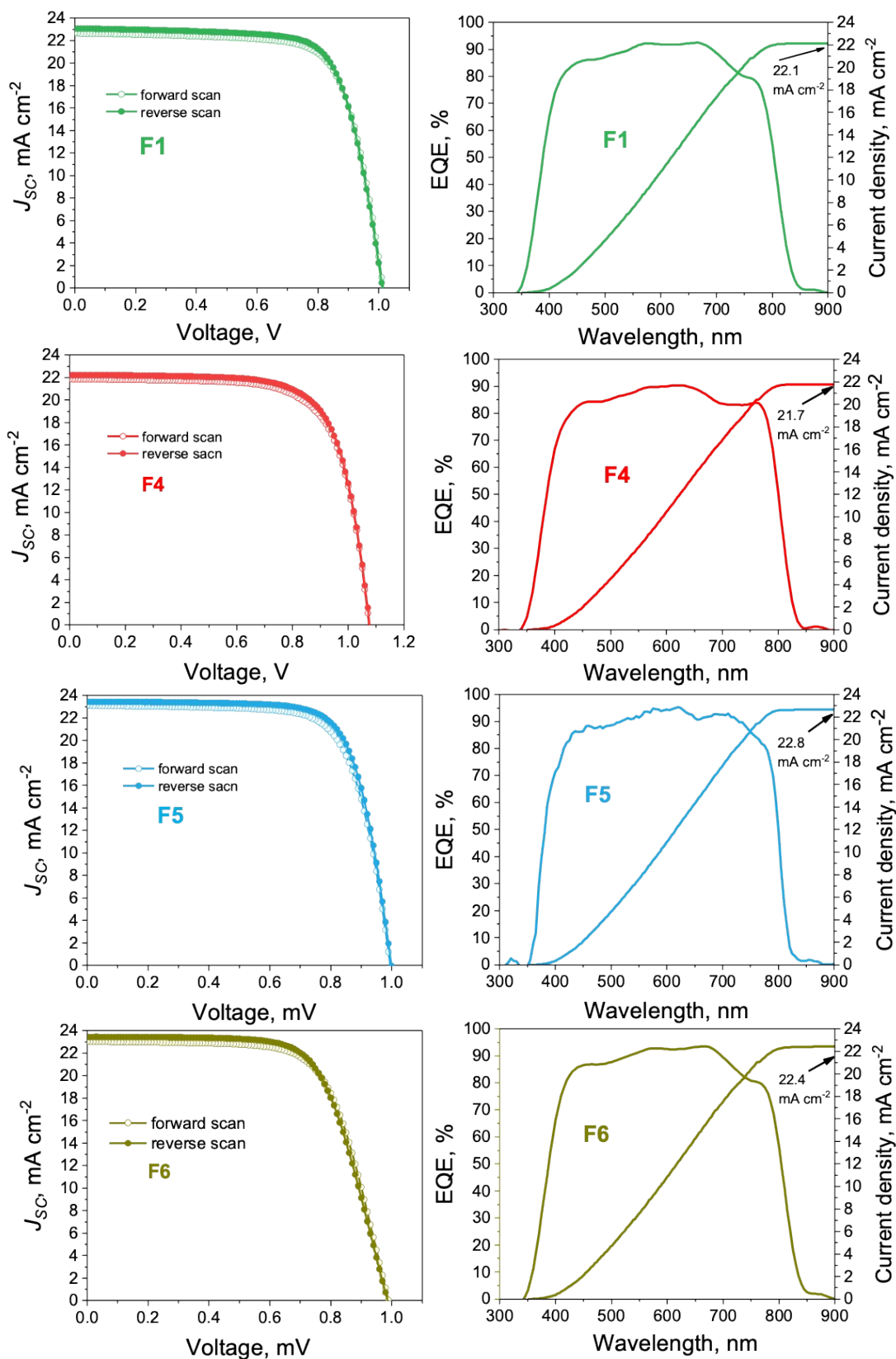


Figure S1. Current density–voltage characteristics (left) and EQE spectra (right) for  $\text{Cs}_{0.12}\text{FA}_{0.88}\text{PbI}_3$ -based PSCs with different ETLs (F1, F4, F5, and F6).

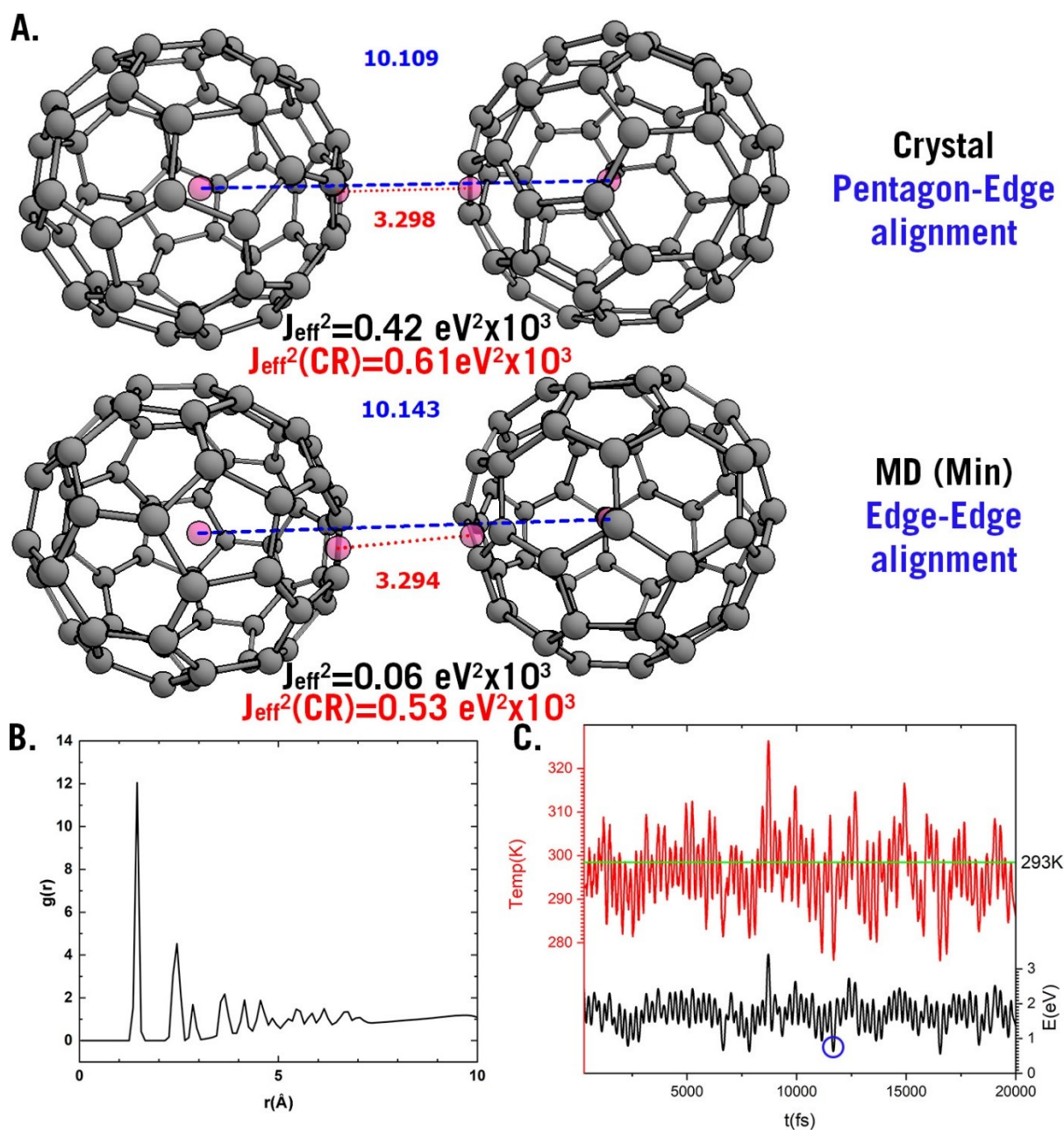


Figure S2. A. Dimer configuration taken from experimental crystals (pentagon-edge) and molecular dynamics minimum (edge-edge). The dotted blue line indicates the distance between the centroids of fullerenes, the red dotted line shows the shortest distance between fullerene surfaces. B. Averaged radial pair distribution function of  $\text{C}_{60}$ . C. Molecular dynamics simulations with a target temperature of 300 K run for 20 ps. CR stands for charge recombination.

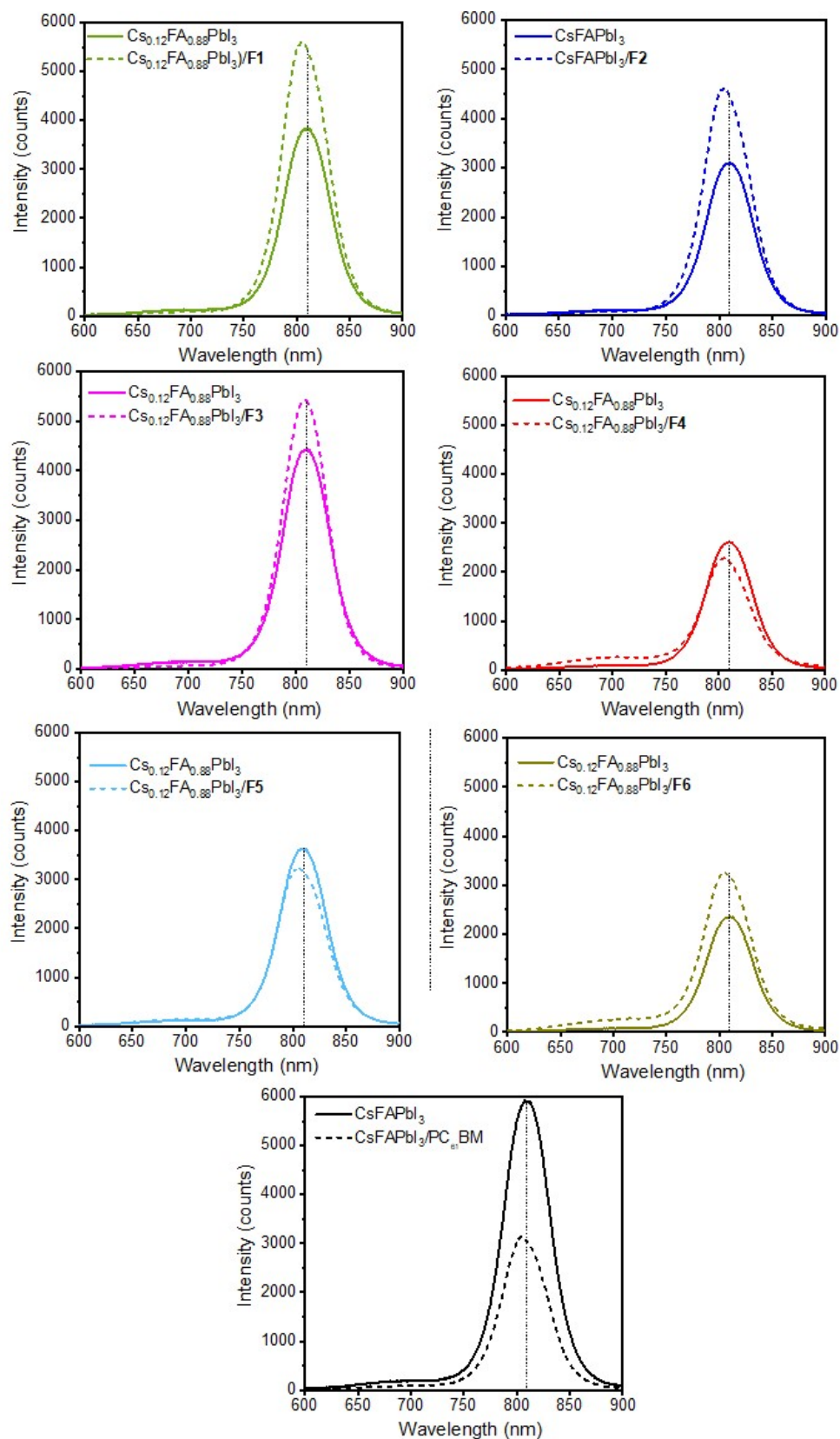


Figure S3. PL spectra of  $\text{Cs}_{0.12}\text{FA}_{0.88}\text{PbI}_3$  films before and after deposition of different fullerene derivatives used as ETL materials.

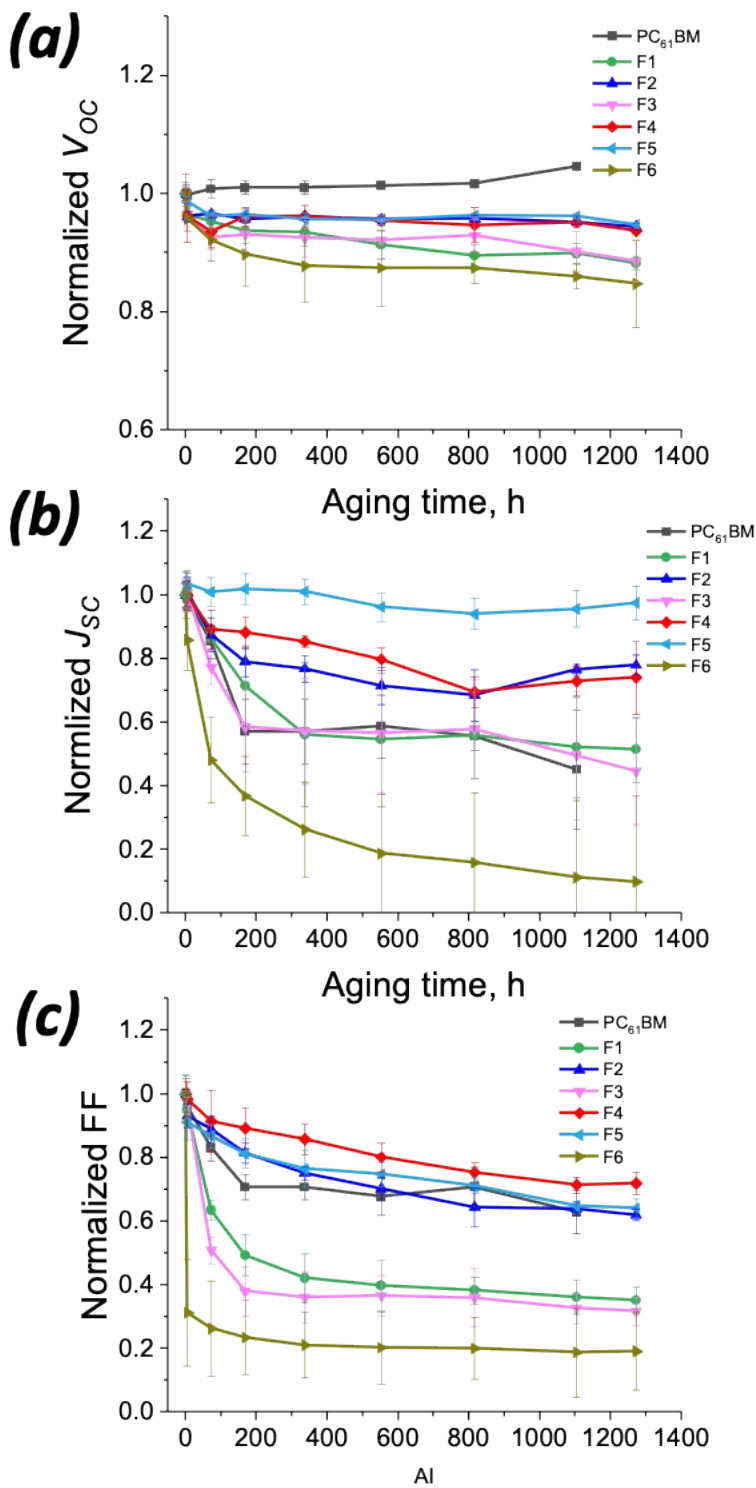


Figure S4. Normalized parameters: (a) open circuit voltage, (b) short circuit current density, and (c) FF for PSCs assembled using different fullerene-based ETLs and exposed to aging under continuous light illumination.

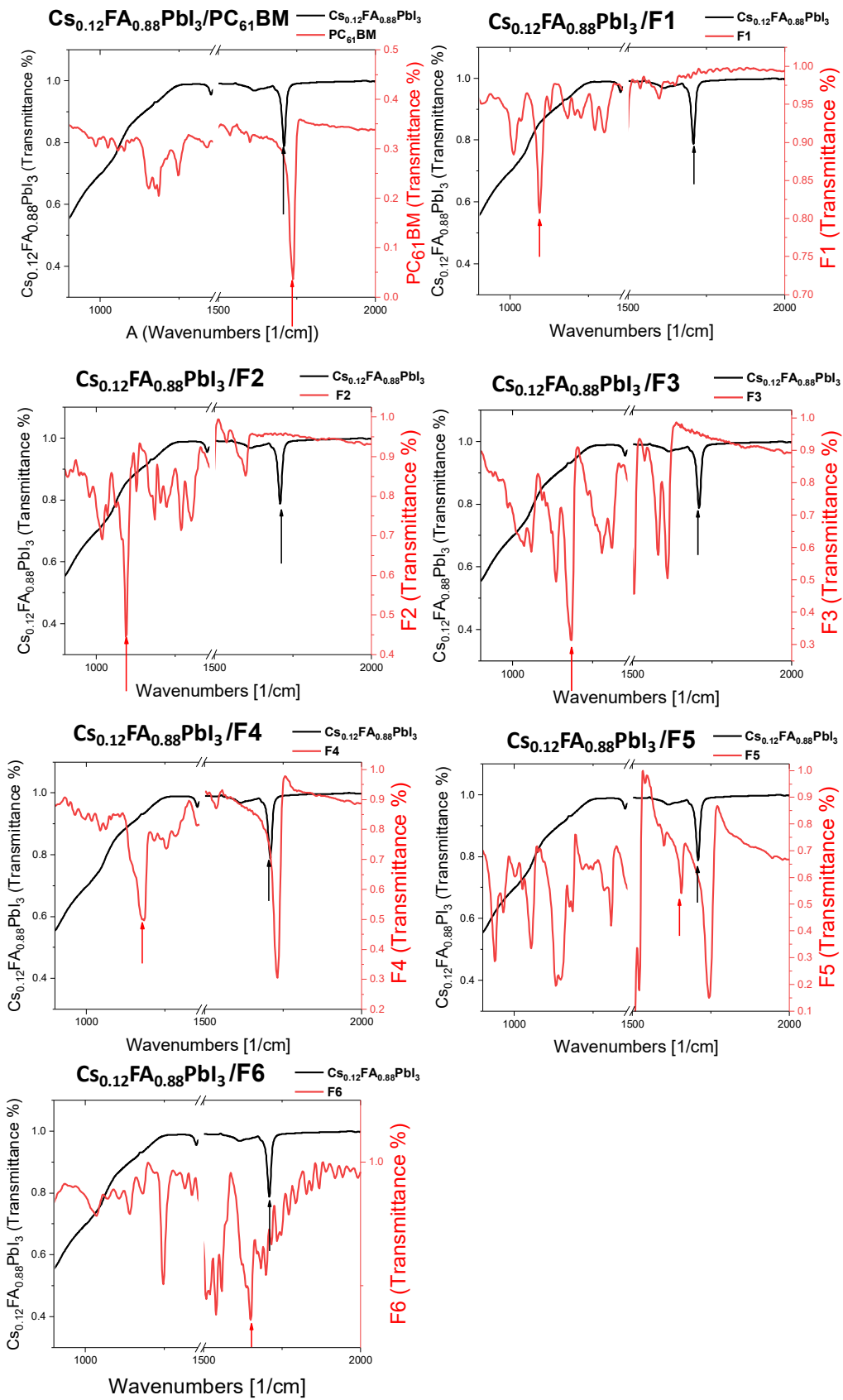


Figure S5. FTIR spectra of  $\text{Cs}_{0.12}\text{FA}_{0.88}\text{PbI}_3$  and fullerene-based ETLs with marked bands used for IR s-SNOM measurements.

## References

- S1 J. C. Hummelen, B. W. Knight, F. Lepeq, F. Wudl, J. Yao and C. L. Wilkins, *J. Org. Chem.*, 1995, **60**, 532–538.
- S2 A. V. Mumyatov, A. E. Goryachev, F. A. Prudnov, O. A. Mukhacheva, D. K. Sagdullina, A. V. Chernyak, S. I. Troyanov and P. A. Troshin, *Synth. Met.*, 2020, **270**, 116565.
- S3 P. A. Troshin, E. A. Khakina, M. Egginger, A. E. Goryachev, S. I. Troyanov, A. Fuchsbauer, A. S. Peregudov, R. N. Lyubovskaya, V. F. Razumov and N. S. Sariciftci, *ChemSusChem*, 2010, **3**, 356–366
- S4 P. A. Troshin, D. K. Susarova, E. A. Khakina, A. A. Goryachev, O. V. Borshchev, S. A. Ponomarenko, V. F. Razumov and N. S. Sariciftci, *J. Mater. Chem.*, 2012, **22**, 18433–18441.
- S5 Sheldrick GM. *Acta Cryst.*, 2008, **A64**, 112-122.
- S6 L. Krause, R. Herbst-Irmer, G. M. Sheldrick and D. Stalke, *J. Appl. Cryst.*, 2015, **48**, 3-10.
- S7. G.M. Sheldrick, *Acta Cryst.*, 2015, **C71**, 3-8.
- S8. M. J. Frisch, G. W. Trucks, H. B. Schlegel, G. E. Scuseria, M. a. Robb, J. R. Cheeseman, G. Scalmani, V. Barone, G. a. Petersson, H. Nakatsuji, X. Li, M. Caricato, a. V. Marenich, J. Bloino, B. G. Janesko, R. Gomperts, B. Mennucci, H. P. Hratchian, J. V. Ortiz, a. F. Izmaylov, J. L. Sonnenberg, Williams, F. Ding, F. Lipparini, F. Egidi, J. Goings, B. Peng, A. Petrone, T. Henderson, D. Ranasinghe, V. G. Zakrzewski, J. Gao, N. Rega, G. Zheng, W. Liang, M. Hada, M. Ehara, K. Toyota, R. Fukuda, J. Hasegawa, M. Ishida, T. Nakajima, Y. Honda, O. Kitao, H. Nakai, T. Vreven, K. Throssell, J. a. Montgomery Jr., J. E. Peralta, F. Ogliaro, M. J. Bearpark, J. J. Heyd, E. N. Brothers, K. N. Kudin, V. N. Staroverov, T. a. Keith, R. Kobayashi, J. Normand, K. Raghavachari, a. P. Rendell, J. C. Burant, S. S. Iyengar, J. Tomasi, M. Cossi, J. M. Millam, M. Klene, C. Adamo, R. Cammi, J. W. Ochterski, R. L. Martin, K. Morokuma, O. Farkas, J. B. Foresman and D. J. Fox, 2016, Gaussian 16, Revision C.01, Gaussian, Inc., Wallingford CT.
- S9 C. Lee, W. Yang and R. G. Parr, *Phys. Rev. B*, 1988, **37**, 785–789.
- S10 J. Da Chai and M. Head-Gordon, *Phys. Chem. Chem. Phys.*, 2008, **10**, 6615–6620.
- S11 S. Grimme, J. Antony, S. Ehrlich and H. Krieg, *J. Chem. Phys.*, 2010, **132**, 154104.
- S12 J. S. Binkley, J. A. Pople and W. J. Hehre, *J. Am. Chem. Soc.*, 1980, **102**, 939–947.
- S13 A. Pal, L. K. Wen, C. Y. Jun, I. Jeon, Y. Matsuo and S. Manzhos, *Phys. Chem. Chem. Phys.*, 2017, **19**, 28330–28343.
- S14 A. Pal, L. K. Wen, C. Y. Jun, I. Jeon, Y. Matsuo and S. Manzhos, *Phys. Chem. Chem. Phys.*, 2017, **19**, 28330–28343.
- S15 P. Piotrowski, W. Mech, K. Zarębska, M. Krajewski, K. P. Korona, M. Kamińska, M. Skompska and A. Kaim, *Molecules* 2021, **26**, 1561.
- S16 E. F. Valeev, V. Coropceanu, D. A. Da Silva Filho, S. Salman and J. L. Brédas, *J. Am. Chem. Soc.*, 2006, **128**, 9882–9886.
- S17 Brown, J. S. (2018). CATNIP (Version 1.9). [Software].
- S18 G. Kresse and J. Hafner, *Phys. Rev. B*, 1994, **49**, 14251–14269.
- S19 S. Grimme, J. Antony, S. Ehrlich and H. Krieg, *J. Chem. Phys.*, 2010, **132**, 10089.
- S20 P. E. Blöchl, *Phys. Rev. B*, 1994, **50**, 17953–17979.
- S21 G. Kresse and D. Joubert, *Phys. Rev. B*, 1999, **59**, 1758–1775.
- S22 J. Sun, R. C. Remsing, Y. Zhang, Z. Sun, A. Ruzsinszky, H. Peng, Z. Yang, A. Paul, U. Waghmare, X. Wu, M. L. Klein and J. P. Perdew, *Nat. Chem.*, 2016, **8**, 831–836.
- S23 H. J. Monkhorst and J. D. Pack, *Phys. Rev. B*, 1976, **13**, 5188-5192.

- S24 L. G. Gutsev, G. L. Gutsev, K. M. Tibbetts and P. Jena, *J. Phys. Chem. A*, 2019, **123**, 9693–9700.
- S25 L. Zhechkov, T. Heine, S. Patchkovskii, G. Seifert and H. A. Duarte, *J. Chem. Theory Comput.*, 2005, **1**, 841–847.
- S26 D. M. Guldi and M. Prato, *Acc. Chem. Res.*, 2000, **33**, 695–703.
- S27 S. Arabnejad, A. Pal, K. Yamashita and S. Manzhos, *Front. Energy Res.*, 2019, **7**, 3